Meteorological analysis of flash floods in Artvin (NE Turkey) on August 24, 2015

Short Title: Meteorological perspective of Artvin flash floods on 24 August 2015

Hakki Baltaci[1*]

[1] Turkish State Meteorological Service, Istanbul, Turkey

* Corresponding author. email: baltacihakki@gmail.com

Tel: +90 2164573400 Fax: +90 2164573403

Abstract

On August 24, 2015 intense rainfall episodes generated flash floods and landslides on the eastern Black Sea coast of Turkey. As a consequence of the heavy rainstorm activity over Artvin and its surroundings (NE Turkey), 11 people died and economic losses totaled a million dollars. During the six hours of the event (from 05:00 UTC to 11:00 UTC), total accumulated rainfall amounts of 136, 64, and 109 mm were measured in the Hopa, Arhavi, and Borçka settlements of Artvin city, respectively. This study comprehensively investigates the meteorological characteristics of those flash floods. In terms of synoptic mechanisms, the cut-off surface low from the summer Asian monsoon settled over the eastern Black Sea. After two days of quasi-stationary conditions of this cyclone, sea surface temperatures (SSTs) reached 27.5 °C (1.5 °C higher than normal) and low-level moisture convergence developed. In addition, transfer of moisture by warm northerly flows from the Black Sea and relatively cool southerly flows from the land coasts of the Artvin district exacerbated the unstable conditions, and thus, played a significant role in the development of deep convective cells. Severe rainstorms as well as the slope instability of the region triggered landslides and worsened flood damages in Artvin area. This study supports conventional weather analysis, satellite images, and forecast model output to alert forecasters to the potential for heavy rainfall.

Keywords: eastern Black Sea; Artvin; flash flood; mesoscale convective systems; Turkey

1. Introduction

The interaction between mesoscale convective systems (MCS) on the warm Mediterranean Sea and sudden orographic lifting in the coastal regions produces severe precipitation in the Mediterranean countries (Rebora et al., 2012). These severe precipitation events generally generate flash floods and cause serious damages and economic losses. For example, just a single flash flood caused 1.2 billion Euro damages in the Gard region of France in 2002 (Huet et al., 2003), 300 million Euro damages in the Pinios (Greece) flash flood during 1994 (Gaume et al., 2008), 65 million Euro economic losses in the Magorala (Spain) flash flood in 2000 (Llasat et al., 2001), and 4.6 million Euro in the 2007 Mastroguglielmo (Italy) flash flood event (Aronica et al., 2008). Due to its huge social and economic impacts, it is necessary to improve our current understanding about the spatio-temporal dynamics of flash floods to improve their forecast and the land-use planning. For this reason, several studies have analyzed the meteorological (e.g. Milelli et al., 2006; Fragoso et al., 2012), hydrological (e.g. Silvestro et al., 2012) or hydrometeorological (e.g. Delrieu et al., 2005; Borga et al., 2007) characteristics of floods at a particular area and time.

Depending on the catchments characteristics, mainly two types of flood occur in Turkey. In the first type, river basins respond rapidly to intense rainfall because of steep slopes, impermeable surfaces, saturated soils, or because of anthropogenic forcing to the natural drainage. As a consequence of this type flooding, large areas are affected, and economic losses are considerable (e.g. the overflow of the Meriç River in NW Turkey). The

second type, which is more common, is when flash floods are suddenly triggered by severe rainstorms in certain areas (e.g. coastal regions of the country). In this context, numerous studies have investigated the meteorological role in the occurrence of flash floods in different parts of Turkey. Kömüşçü et al. (1998) analyzed the meteorological and terrain features of the flash flood that occurred on November 3 and 4, 1995 on the Aegean coast, when 61 people died in İzmir (western Turkey). They emphasized that low-level advection, positive vorticity, and strong upper-level divergence together with a squall line oriented NE-SW over the Aegean Sea exacerbated the storm. Subsequently, Kotroni et al., (2006) investigated the storm activity that occurred on December 5, 2002 in Antalya, a coastal city located on the Mediterranean Sea. They found that warm and moist air masses driven by a low-level jet as well as orographic barriers caused more than 230 mm of 24-h accumulated precipitation during the event. Later, Kömüşcü and Çelik (2013) investigated the hydrometeorological role of floods occurred during 7-10 September, 2010 in the Marmara Region. They concluded that cold air in the upper atmosphere, slow-moving quasi-stationary trough and continuous moisture transfer from the warm Aegean Sea to the surface low were the main mechanisms that led to intense storms.

Differently from the previous studies mentioned above, many severe precipitation events frequently occur and generally conclude with flash floods and triggered landslides in the eastern Black Sea (EBS) region of Turkey (Fig. 1). The EBS comprises the Black Sea (BS) in the north and the eastern Anatolian Peninsula in the south. The underlying geology of the EBS is generally consists of semi-permeable volcanic rocks which reduce infiltration and enhance runoff production (Üçüncü et al., 1994). The north-eastern coastal parts of Turkey, regions located on the windward slopes of the EBS facing the Black Sea, receives

more than 2000 mm of annual precipitation which is the wettest part of the country. The large mountainous area which extends through the Black Sea, and slope instability due to steep gradients as well as intense rainfall result in flash floods and landslides and threaten the settlements in the EBS region. In addition to all these topographical and meteorological factors, commercial development and urbanization of the region (e.g. the cultivation of tea on the sloping terrain instead of deep-rooted trees and illegal land-usage) facilitate the flooding. Yüksek et al., (2013) have emphasized that 258 deaths and US $500,000,000 economic losses occurred as a result of the 51 big floods in this basin from 1955 to 2005. They briefly analyzed the hydro-meteorological role of selected nine floods in the region. In one of the latest rainstorm events in the EBS, more than 135 mm of 24-h accumulated rainfall in the Artvin surroundings (i.e. 144, 136 and 149 mm in Hopa, Arhavi and Borçka stations, respectively) caused flash floods and landslides on August 24, 2015, resulting in 11 deaths and a million dollars worth of economic losses (Fig. 2). In spite of the several negative impacts of flooding for the region and country, there are no detailed studies in the literature which investigate the detailed meteorological role in the development of the convective cells for the EBS. Therefore, the aim of this research is focused on this extreme event, with the following main objectives: (a) to provide a detailed spatio-temporal evaluation of rainstorms on 24 August 2015 that triggered the flash floods and landslides. Daily and hourly precipitation measurements of the available meteorological stations were used to understand temporal and spatial behavior of the rainstorm in the different geographic elevations, (b) to improve our understanding of the meteorological features of this extreme event by focusing on the relevant atmospheric synoptic conditions, satellite

and radar images and physical mechanisms (e.g. sea surface temperature evolution) that favored its development.

2. Data and Methodology

In order to evaluate the research results, precipitation, sea surface temperature, synoptic, and atmospheric data are included in the study. To compare precipitation observations with weather forecasts, three numerical weather prediction (NWP) model outputs were assessed.

2.1 Precipitation and sea surface temperature (SST) data

The eastern Black Sea region is well covered by automated meteorological stations. In addition to the eight long-term stations in the region, 41 new automated meteorological stations have been added since 2013. To present the high spatial resolution and to retrieve a homogeneous dataset, hourly and daily precipitation data of 49 stations operated by Turkish State Meteorological Service (TSMS) were used in the study (Fig.1). The main characteristics of the stations are described in Table 1.

2.2 Synoptic and atmospheric data

The synoptic context of the extreme event of August 24, 2015 as well as the previous day atmospheric conditions was analyzed with NCEP/NCAR 2.5°X2.5° latitude/longitude reanalysis data. To track the intense rainfall episodes, radar PPI (Plan Position Indicator) images, which provided by TSMS, were used. Rainstorm development stages associated with the flash flood were evaluated with Meteosat 10 images.

2.3 Numerical weather prediction (NWP) model outputs

Operationally, one global and two regional NWP models are run regularly twice a day (00:00 and 12:00 UTC) for the precipitation forecast by TSMS. In terms of the global NWP, the horizontal grid resolution of ECMWF (European Centre for Medium-Range Weather Forecasts) the IFS (Integrated Forecast System) covers almost 16 km and uses 91 vertical levels. For the regional weather forecasts, the Alaro meteorological model has been designed to be run at convection-permitting resolutions. The key concept is in the precipitation and cloud scheme called Modular Multiscale Microphysics and Transport (3MT) developed by Gerard and Geleyn (2005), Gerard (2007), and Gerard et al. 2009. In the usage of the Alaro by TSMS whereas the outer domain has grid spacing of 10 km, the inner domain has almost 5 km of grid spacing as well as 60 vertical levels.

The mesoscale NWP system of Non-hydrostatic Mesoscale Model (NMM) core of the Weather Research and Forecasting (WRF) is developed by the National Oceanic and Atmospheric Administration (NOAA)/National Centers for Environment Prediction (NCEP), WRF-NMM is a fully compressible, non-hydrostatic mesoscale model with a hydrostatic option (Janjic, 2003). The model uses a terrain-following hybrid sigma-pressure vertical coordinate. The grid staggering is the Arakawa E-grid. The model uses a forward-backward scheme for horizontally-propagating fast waves, an implicit scheme for vertically-propagating sound waves, the Adams-Bashforth scheme for horizontal advection, and the Crank-Nicholson scheme for vertical advection. The dynamics conserve a number of first and second order quantities including energy and enstrophy. In the study, model has a horizontal grid spacing of 30 km in its outer computational domain, and the inner domain

has a grid spacing of 10 km together with 46 vertical levels. To compare precipitation forecasts of these models with the observation results, daily precipitation forecasts of the models belonging on the last runtime for August 24, 2015, at 00:00 UTC outputs were assessed.

3. Results and discussion

3.1 Precipitation climate of eastern Black Sea

The coastal part of the region is restricted by the EBS Mountain chain in the south and the BS in the north (Fig.1). This mountain chain extends parallel to the Black Sea and has an average altitude of 2000 m. It rises to 3973 m at its highest point (Eris et al., 2012). Apart from the basic synoptic scale circulations such as continental polar and tropical air masses, the region is also affected by orographic precipitation. Colder air masses are prevented by the Caucasus Mountains (the highest point of Georgia) from the north; therefore, more dry climates are seen in the south part of the region. The rain shadow effect on the lee side of the mountainous area causes a more continental climate in the southern parts of the EBS (Biyik et al., 2010). When compared with the other regions, highest winter and summer precipitation totals are observed in this part of Turkey due to the interactions of synoptic weather patterns and orographic lifting. (Unal et al., 2012). To better visualize the seasonal precipitation variability in the EBS, long-term precipitation data from 1960 to 2014 were extracted from the available eight meteorology stations (stations marked by stars in Table 1 were used for the climatological approach in Fig. 3). Five stations are located in the north of the region. According to the results, mean annual precipitation (MAP) varies from 438

mm in the south (Bayburt) to 2243 mm in the north (Hopa). This high spatial precipitation variability generates different land cover terrain. Interestingly, the highest seasonal precipitation amounts in the coastal areas were observed in the fall (SON) months. This can be explained by the significance of MCS, flow directions and SST variations over EBS. In the second wettest season (DJF), highest precipitation records were observed at Hopa, Rize, and Pazar stations with the values 606, 636, and 550 mm, respectively.

3.2 Spatio-temporal variability of rainfall episodes

In Fig. 4a, spatial distribution of daily precipitation totals for August 24, 2015 was extracted from 49 meteorological stations. It can be seen that three main cores of precipitation are measured at the Arhavi, Hopa, and Borçka stations with the values of 135, 144, and 149 mm, respectively. In Hopa, 27% of the long-term mean of summer rainfalls was recorded on this day. As a consequence of the intense daily rainfall episodes, these three surrounding areas of Artvin district were the most influenced by flash floods and landslides (i.e. Hopa, Arhavi, and Borçka). Among these stations, Hopa (33m altitude, no. 1 in Fig. 1b) is at the lowest altitude and is located in the north coastal part of Artvin city. Borçka station is shown with an altitude of 190m (the second lowest altitude in Artvin, no. 7 in Fig. 1b). Another coastal station, Arhavi (290m altitude, no. 6 in Fig 1b), is located in the northwest and has the third lowest altitude among all Artvin stations. Temporal precipitation distribution of these selected stations was extracted as shown in Fig. 4b. Rainstorms started in the evening (22:00 UTC) of August 23, 2015 and ended at the midday on the following day. Hourly observations at the three stations showed the torrential rains increased from 27 to 32 mm between 22:00 and 24:00 UTC on August 23,

thereafter suddenly dropping from 4 to 2 mm between 01:00 and 05:00 UTC on August 24. Later, uninterrupted extreme rainstorms hit the north and coasts of the Artvin district. According to the hourly rainfall observations, the highest precipitation amounts were recorded at Hopa during the eight hours of the flash flood day (Fig. 4b). The maximum daily precipitation value was observed with 144.3 mm in six hours (starting at 05:00 UTC and ending at 11:00 UTC) in Hopa, and maximum hourly rainfall measured 51.5 mm at 09:00 UTC. In Arhavi, daily total precipitation was 135.5 mm and reached a maximum value at 00:00 UTC with 32.4 mm. In Borçka, while daily precipitation amounts were higher (148.9 mm) than at Hopa and Arhavi, peak values of hourly precipitation intensities were lower. According to the results from these three stations, hourly precipitation reached a maximum value at 09:00 UTC in the low altitudes of the region; this implies that the precipitation was much lower in the upper sectors of the mountainous area.

3.3 Synoptic overview

This section treats the atmospheric circulation and associated physical mechanisms that were responsible for the flash flood in the region. In order to better evaluate the phenomenology of the event, pre-existing synoptic conditions starting from August 23 were investigated. At 00:00 UTC on August 23, the summer Asian monsoon low extends to the eastern Black Sea (Fig. 5a). During the summer months, in consequence of the excessive surface heating over the arid regions of the Middle East, the monsoon low expands westward and generates the Persian trough (Alpert et al. 2004; Saaroni et al. 2010), which extends to Turkey, forming a thermal low over the eastern Mediterranean (Tyrlis et al. 2015). Besides the surface synoptic conditions, low-level moisture convergence, specific

208 humidity content and geopotential height values of 850 hPa were extracted. It is known that
209 low-level moisture convergence is a good indicator for large-scale precipitation (e.g.
210 Fragoso et al. 2012), and eastern Turkey (Azerbaijan) has good synoptic precipitation
211 conditions. In the upper levels, interaction between weak ridge over northern Africa and
212 trough over the Aegean Sea (because of the upper-level cold low over central Europe)
213 concludes with southwesterly winds over the Artvin district (Fig. 5c).

214 On August 24 at 00:00 UTC, a high pressure center (HPC) over northern Russia moved to
215 the south, located around 30° E, 60° N. While the cyclone remained almost stationary, a
216 new cut-off cyclone occurred over the EBS (Fig. 5d). Thus, high northeasterly winds
217 brought moisture from the Black Sea to the eastern coasts of Turkey (Fig. 5e). As a result,
218 deep precipitation areas were observed over these regions according to the low-level
219 moisture convergence results. In the upper level chart (500 hPa), shifting cold core of upper
220 level high to the south cause the moving of mid-latitude low to the west, and, thus south-
221 westerly winds turn into the westerly together with a decrease in temperature from -7.5 °C
222 to -10 °C (Fig. 5f).

223 At the start of the rainstorm (August 24, 06:00 UTC), similar surface and upper-level large-
224 scale circulations appeared compared with the midnight synoptic conditions (Figs 6a and
225 6c). Strong moisture convergence zones were detected over the flash-flood region (Fig. 6b).
226 For this reason, thermodynamic analysis was needed to better understand the evaluation of
227 physical mechanisms that developed severe precipitation. Hence, as a consequence of
228 analyzing the nearest radiosonde measurements from Samsun station (41.34 °N, 36.25 °E),

instability indices such as CAPE (Convective Available Potential Energy) and LI (Lifted Index) showed that there was no strong convective activity before and during the rainstorm (not shown).

In order to follow the distribution convective cells and cloud droplets in a large area, it was necessary to use satellite and radar image data.

3.4 Satellite and radar images

Repeated temporal resolution is an excellent tool for understanding the spatial distribution of the convective cells. Therefore, SEVIRE (Spinning Enhanced Visible and Infrared Imager) MSG (Meteosat Second Generation) outputs were used to examine the atmospheric conditions on August 24 at 06:00 UTC. It is known that 'convective storms RGB' product visualizes the particle size features of high-level cloud tops with good contrast (Kerkmann et al., 2006). Whereas yellowish cloud tops indicate opaque ice clouds with small particles, high-level opaque ice clouds with large particles are shown as reddish. The RGB product in Fig. 7a was produced by assigning the brightness temperature difference (BTD) 6.2-7.3 values as the red component, the BTD 3.9-10.8 as the green component, 1.6-0.6 as the blue component. In Fig. 7a, numerous convective storms with large ice particles are shown over the EBS. On the other hand, more intense storms were observed over the land areas such as Georgia and this implies the storm intensity. Separately, SYNOP observations indicate that southerly winds over the coast of the EBS stations met with humid northerly flows throughout the seaside area. If the land (21 °C) and sea surface temperatures (SSTs) were sufficiently different, the convective instability and storm severity could have increased

250 with time. As seen in Fig. 7b, high PPI (Plan Position Indicator) reflectivity values from the
251 radar image showed that two cores of the extreme precipitation were over the Hopa and
252 Çayeli sub-basins.

253 **3.5 Sea surface temperature (SST) analysis over Black Sea**

254 The influence of SSTs on precipitation over Turkey was investigated in detail by Bozkurt
255 and Sen (2011). They found that increased SSTs led to increased precipitation of the
256 peninsula especially downwind of the sea. Later, Kömüşçü and Çelik (2013) explained that
257 warm Aegean SST is one of the significant causes of the development of rainstorms. In this
258 study, exploring the role of Black Sea surface temperatures on storm development, long-
259 term (1982-2015) means of August SSTs were extracted for the BS using NOAA High
260 Resolution SST data (provided by NOAA/OAR/ESRL PSD, Reynolds et al. 2007). As seen
261 in Fig. 8a, cold SSTs of the BS were north of the latitude of 44 °N. The warmest pool of the
262 BS in the eastern BS and SSTs exceeded 27 °C in this month. During the day of the
263 extreme event, spatial distribution of the SSTs indicates negative anomaly values in north
264 of 44 °N latitudes (Fig. 8b). The EBS region has the highest SST anomalies and 1.5 °C
265 higher SST variations compared with the August means for the EBS.

266 **3.6 Forecasting tools: Numerical Weather Prediction (NWP) models**

267 According to the ECMWF daily precipitation product, spatial coverage of the maximum
268 daily precipitation values (over 160 mm) is shown in the northern Rize and northwestern
269 Artvin cities (Fig. 9a). Compared with the model output (Fig. 4a), station observations were
270 clearly underestimated in northern Rize. On the other hand, model predictions for the

Arhavi and Borçka settlements, except Hopa, were good. With regard to the Alaro model results, the highest daily precipitation totals were well predicted only for Hopa district at 150 mm (Fig. 9b). Although precipitation forecasts of this limited-area model described Hopa well, the other two flood regions were not well predicted. Optimum spatial coverage of the daily precipitation forecasts is shown in the mesoscale WRF outputs (Fig. 9c). The problem with this model is the underestimated forecasts compared with the observation data. In TSMS, meteorologists merge the outputs of these models (the so-called "poor man ensemble") with their own experience and provide quantitative precipitation forecasts for the alert sub-regions in predefined time windows. As a consequence of this subjective prediction, TSMS and its regional weather forecast offices issued alert messages related to natural hazards including severe precipitation events. These organizations also carry the responsibility for nowcasting and monitoring rainfall events. According to the main alert on August 23, 2015 at 09:00 UTC prepared by TSMS Weather Forecast Centre, very intense precipitation between 51 and 100 mm was predicted at the Rize, Artvin, and Trabzon districts within 12 hours of August 24. The authorities and the public were alerted to the risk of flash flood, lightning, and landslide events.

4. CONCLUSION

This paper investigated the meteorological role in an extraordinary rain event over Artvin. The flooding event on August 24, 2015 that hit the Artvin area has been analyzed from a meteorological perspective. A large amount of precipitation fell in an area of a few square kilometers with high intensity in about 6 to 7 hours, and NWP models cannot well predict such extreme events. Although alert messages were prepared by TSMS on August 23 at

09:00 UTC, 11 people died and infrastructures, buildings, private property and public goods were damaged as a result of the flash flood.

According to the synoptic conditions, when the summer monsoon frontal system extended to eastern Anatolia, its activity was enhanced. On the other hand, because of the depressive effect of the Siberian high from the north, a cut-off low occurred over the eastern Black Sea. As a result, a slow-moving quasi-stationary cut-off low over the Black Sea increased the SSTs and more moisture was transported from the sea to the atmosphere. Thus, strong moisture convergence at low-levels (850 hPa) was observed over Artvin city. Moreover, warm humid northerly airs from the Black Sea and relatively cool southerly flows (21 °C) over the land areas increased the instability conditions and redevelopment of the convective cells over the same region enhanced the rainfall intensity.

The synoptic and atmospheric descriptions give better knowledge of the mesoscale convective systems and the mechanisms driving torrential rains in the EBS. It is hoped that more detailed studies will be performed on synoptic development leading to extreme summer precipitation events in EBS.

References

Alpert, P., Osetinsky, I., Ziv, B. and Shafir. H.: A new seasons definition based on classified daily synoptic systems: an example for the eastern Mediterranean. International Journal of Climatology 24:1013–1021, 2004.

Aronica, G.T., Brigandi, G., Marletta, C. and Manfre, B.: Hydrological and hydraulic analysis of the flash flood event on 25 October 2007 in North-Eastern part of Sicily, Italy. Proceedings of Floodrisk 2008, Oxford (UK), 2008.

Arpe, K., Dümenil, L. and Giorgetta, M. A.: Variability of Indian Monsoon in the ECHAM3 Model: sensivity to sea surface temperature, soil moisture, and stratospheric quasi-biennial oscillation. Journal of Climate 11:1837–1858, 1998.

Biyik, G., Unal, Y. S. and Onol, B.: Assessment of Precipitation Forecast Accuracy over Eastern Black Sea Region using WRF-ARW. European Geosciences Union General Assembly, Vienna, 02.05.2010–07.05.2010, 2010.

Borga, M., Boscolo, P., Zanon, F. and Sangati, M.: Hydrometeorological Analysis of the 29 August 2003 Flash Flood in the Eastern Italian Alps. Journal of Hydrometeorology 8: 1049–1067, 2007.

Bozkurt, D. and Sen, O. L.: Precipitation in the Anatolian Peninsula: sensitivity to increased SSTs in the surrounding seas. Climate Dynamics 36: 711–726, 2011.

Delrieu, G., Nicol, J., Yates, E., Kirstetter, P. E., Creutin,, J. D., Anquetin, S., Obled, C. H., Saulnier, G. M., Ducrocq, V., Gaume, E., Payrastre, O., Andrieu, H., Ayral, P. A., Bouvier, C., Neppel, L., Livet, M., Lang, M., Parent du-Châtelet, J., Walpersdorf, A. and Wobrock, W.: The catastrophic flash-flood event of 8–9 September 2002 in the Gard region, France. A first case study for the Cévennes–Vivarais mediterranean hydrometeorological observatory. Journal of Hydrometeorology 6 (1):34–52, 2005.

Eris, E. and Agiralioglu, N.: Homogeneity and Trend Analysis of Hydrometeorological Data of the Eastern Black Sea Region, Turkey. Journal of Water Resource and Protection 4:99–105, 2012.

Fragoso, M., Trigo, R. M., Pinto, J. G., Lopes, S., Lopes, A., Ulbrich, S. and Magro, C.: The February 2010 Maderia flash-floods: synoptic analysis and extreme rainfall assessment. Natural Hazards and Earth System Sciences 12:715–730, 2012.

Gaume, E., Bain, V. and Bernardara, P.: Primary Flash flood Data, Work Package 1 Report for HYDRATE, EC Project No. GOCE-CT-2004-505420, 2008.

Gerard, L.: An integrated package for subgrid convection, clouds and precipitation compatible with the meso-gamma scales. Quarterly Journal of the Royal Meteorological Society 133:711–730, 2007.

Gerard, L. and Geleyn J. F.: Evolution of a subgrid deep convection parameterization in a limited area model with increasing resolution. Quarterly Journal of the Royal Meteorological Society 131:2293–2312, 2005.

Gerard, L., Piriou J. M., Brozkova, R., Geleyn, J. F. and Banciu, D.: Cloud and precipitation parameterization in a meso-gamma-scale operational weather prediction model. Monthly Weather Review 137: 3960–3977, 2009.

Huet, Ph., Martin, X., Prime, J-L., Foin, P., Laurain, C. I. and Cannard, Ph.: Retour d'expe´riences des crues de septembre 2002 dans les de´partements du Gard, de l'He´rault, du Vaucluse, des bouches du Rho^ne, de l'Arde`che et de la Dro^me, Inspection ge´ne´rale de l'Environnement, Paris, France, 124 pp, 2003.

Janicot, S., Harzallah, A., Fontaine, B. and Moron, V.: West African monsoon dynamics and Eastern Equatorial Atlantic and Pacific SST anomalies (1970-1988). Journal of Climate 11:1874–1882, 1998.

Janjic Z. I.: A nonhydrostatic model based on a new approach. Meteorology and Atmospheric Physics 82: 271–285, 2003.

Kerkmann, J., Lutz, H. J., König, M., Prieto, J., Pylkko, P., Roesli, H. P., Rosenfeld, D. and Zwatz-Meise, G.: 20060 MSG Channels, Interpretation Guide, Weather, surface Conditions and Atmospheric Constituents. *Available online at http://oiswww.eumetsat.org/WEBOPS/msg_interpretation/index.html,* 2006.

Kotroni, V., Lagouvardos, E., Defer, S., Dietrich, F., Porcu, C., Medaglia, C. M. and Demirtas, M.: The Antalya 5 December 2002 Storm: Observations and Model Analysis. Journal of Applied Meteorology and Climatology 45:576–590, 2006.

Kömüşçü, A. Ü., Erkan, A. and Çelik, S.: Analysis of Meteorological and Terrain Features Leading to the İzmir Flash Flood, 3–4 November 1995. Natural Hazards 18:1–25, 1998.

Kömüşçü, A. Ü. and Çelik, S.: Analysis of the Marmara flood in Turkey, 7–10 September 2009: an assessment from hydrometeorological perspective. Natural Hazards 66:781–808, 2013.

LLasat, M. C., De Batlle, J., Rigo, T. and Barriendos, M.: Las Inundaciones del 10 de Junio del 2000 en Catalana. Revista Ingenieria del Agua 8: 53–66, 2001.

Maracchi, G., Crisci, A., Grifoni, D., Gozzini, B. and Meneguzzo, F.: Relationships between convective events and sea surface temperature anomalies in coastal regions of the Mediterranean. Proceedings of the EuroConference on global change and catastrophe risk management: flood risks in Europe. Laxenburg, Austria, 1999.

Messager, C., Gallee, H. and Brasseur, O.: Precipitation sensitivity to regional SST in a regional climate simulation during the West African monsoon for two dry years. Climate Dynamics 22:249–266, 2004.

Milelli, M., Llasat, M. C. and Ducrocq, V.: The cases of June 2000, November 2002 and September 2002 as examples of Mediterranean floods. Natural Hazards and Earth System Sciences 6:271–284, 2006.

Rebora, N., Molini, L., Casella, E., Comellas, A., Fiori, E., Pignone, F., Siccardi, F., Silvestro, F., Tanelli, S. and Parodi, A.: Extreme Rainfall in the Mediterranean: What Can We Learn from Observations?. Journal of Hydrometeorology 14: 906–922, 2013.

Reynolds, R. W., Smith, T. M., Liu, C., Chelton, D. B., Casey, K. S. and Schlax, M. G.: Daily high-resolution-blended analyses for sea surface temperature. Journal of Climate 20:5473–5496, 2007.

Saaroni, H., Ziv, B., Osetinsky, I. and Alpert, P.: Factors governing the interannual variation and the long-term trend of the 850 hPa temperature over Israel. Quarterly Journal of the Royal Meteorological Society 136:305–318, 2010.

Silvestro, F., Gabellani, S., Giannoni, F., Parodi, A., Rebora, N., Rudari, R. and Siccardi, F.: A hydrological analysis of the 4 November 2011 event in Genoa. Natural Hazards and Earth System Sciences 12:2743–2752, 2012.

Tyrlis, E., Tymvios, F. S., Giannakopoulos, C. and Lelieveld, J.: The role of blocking in the summer 2014 collapse of Etesians over the eastern Mediterranean. Journal of Geophysical Research: Atmospheres 120: doi:10.1002/2015JDO23543, 2015.

Unal, Y. S., Deniz, A., Toros, H. and Incecik, S.: Temporal and spatial patterns of precipitation variability for annual, wet, and dry seasons in Turkey. International Journal of Climatology 32:392–405, 2012.

Üçüncü, O., Önsoy, H. and Yüksek, Ö.: A Study on the environmental effects of 20 June 1990 flood in Trabzon and its neighborhood, Turkey. 2nd International Conference on River Flood Hydraulics. York, England, 1994.

Yüksek, Ö., Kankal, M. and Üçüncü, O.: Assessment of big floods in the Eastern Black Sea Basin of Turkey. Environmental Monitoring and Assessment 185:797–814, 2013.

418 **Table 1 :** Description of 49 meteorological stations in the study. Stations marked by stars
419 were used for the climatological approach.

Station No.	Station Code	Station name	Longitude (E)	Latitude (N)	Altitude (m)	23 Aug 2015 precip. (00-00 UTC)	24 Aug 2015 precip. (00-00 UTC)
1	17042	Hopa*	41.4330	41.4065	33	55.3	144.3
2	17045	Artvin*	41.8187	41.1752	613	0	1.4
3	18216	Yusufeli	41.5464	40.8228	601	0	4.4
4	18217	Savsat	42.3206	41.2433	1125	0	24.4
5	18218	Ardanuc	42.0653	41.1267	577	0	11.6
6	18554	Arhavi	41.2928	41.3166	290	22.4	135.5
7	18555	Borcka	41.6281	41.3750	190	35.8	148.9
8	18556	Murgul	41.5564	41.2617	565	0.2	42.5
9	17089	Bayburt*	40.2207	40.2547	1584	0.4	0
10	18219	Demirozu	39.8858	40.1639	1757	0	0
11	18557	Aydintepe	40.1294	40.3817	1600	0.6	0
12	17088	Gumushane*	39.4653	40.4598	1216	0.1	0
13	17696	Torul (Zigana kayak m)	39.4037	40.6413	2050	0	0
14	18226	Kurtun	39.1456	40.6825	739	0	1.5
15	18227	Torul	39.2989	40.5686	1009	0	0
16	18228	Kelkit	39.4361	40.1506	1483	0	0
17	18564	Kose	39.6578	40.2217	1635	0.1	0
18	18565	Siran	39.1289	40.1856	1490	3.3	0
19	17040	Rize*	40.5013	41.0400	3	28.3	26.2
20	17628	Pazar*	40.8993	41.1777	78	35.8	49
21	17713	Camlihemsin (Ayder Fl)	41.1103	40.9518	1354	1.6	18.8
22	17741	Ikizdere (Sivrikaya)	40.7106	40.6711	1926	0	7.8
23	17757	Ikizdere (Derekoy)	40.5989	40.7258	970	0.4	37.2
24	17761	Kalkandere	40.4400	40.9278	138	5.7	75.1
25	17765	Camlihemsin	40.9942	41.0125	390	2.8	32.1
26	17769	Hemsin	40.8992	41.0503	307	22.3	21.9
27	17772	Ardesen (Yesiltepe)	41.0703	41.1528	573	0.4	0
28	17775	Iyidere (Fidanlik)	40.3319	40.9835	6	21.1	29.8
29	17781	Cayeli (Teias)	40.7417	41.0603	54	31.9	30.9
30	17785	Cayeli (Kaptanpasa)	40.7789	40.9583	483	15.2	54.1
31	17800	Guneysu	40.6083	40.9897	124	31.1	58.8
32	18566	Derepazari	40.4289	40.9897	397	20.1	38
33	18567	Findikli	41.1556	41.2703	190	24.7	62.3
34	18568	Rize (Andon)	40.5825	40.8711	615	12.6	88.8
35	18569	Ikizdere (Cimil)	40.7828	40.7333	2020	0.5	16.3
36	18905	Cayeli (Bakir)	40.7669	41.0408	100	32.3	56.5
37	17037	Trabzonbolge*	39.7649	40.9985	25	2.6	17.4
38	17569	Caykara (Uzungol)	40.4435	40.6193	1114	1.6	11.6
39	17626	Akcaabat*	39.5615	41.0325	3	1	36.6
40	17714	Macka (Altindere sume.)	39.6532	40.6985	1030	0.4	1.6
41	18229	Duzkoy	40.1339	40.7708	622	0.7	8.2
42	18230	Tonya (Kalincam)	39.2617	40.7803	1100	0	7.1
43	18231	Besikduzu	39.2144	41.0328	374	12	30.1

44	18232	Hayrat (Pazaronu)	40.4961	40.8858	367	17.6	43
45	18233	Arsin	39.9497	40.9486	169	0	14.5
46	18570	Dernekpazari	40.2719	40.7997	721	7	9.7
47	18571	Koprubasi (Beskoy)	40.1339	40.7710	975	14	17.3
48	18573	Carsibasi (Yoroz)	39.4208	41.0950	370	1.2	47.8
49	18574	Surmene (Denizbilimleri)	40.2097	40.9231	5	49.5	33.8

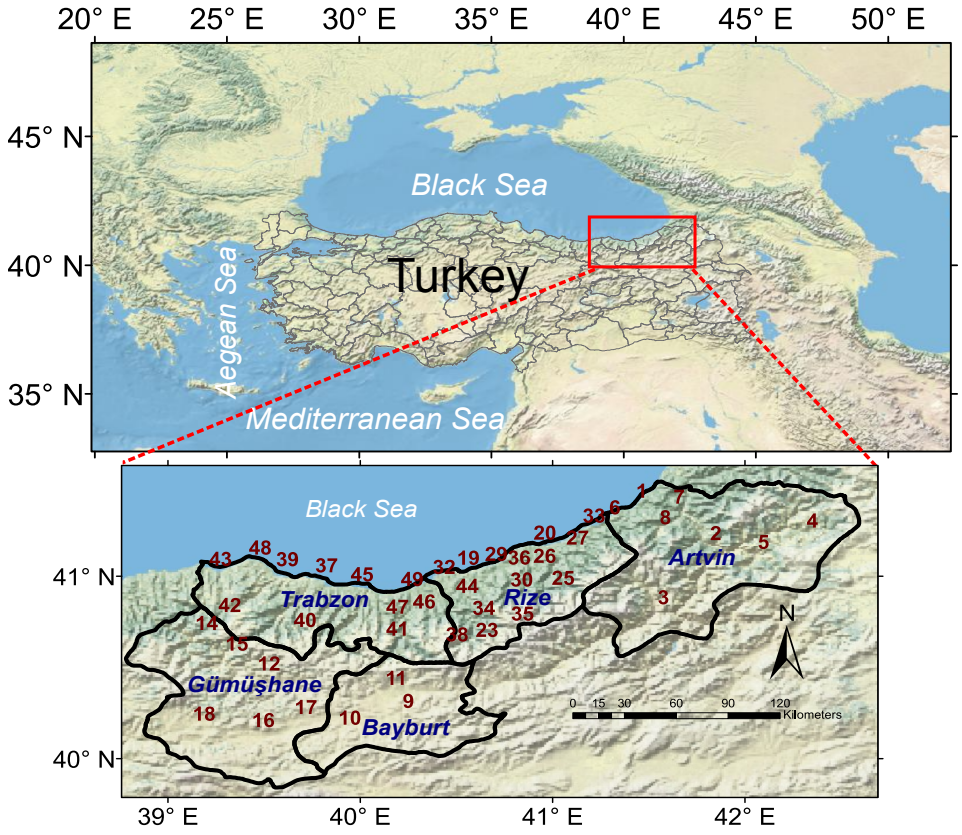

Figure 1. The eastern Black Sea Region included city names and borders and 49 automated meteorological stations (Descriptions of the station numbers are explained in Table 1). The outset shows location of the region in Turkey.

(a) (b)

Figure 2. Photos showing the destructive effects of the 24 August 2015 flash-floods and landslides in: **(a)** Hopa city centre flash-flood and **(b)** landslide in Hopa

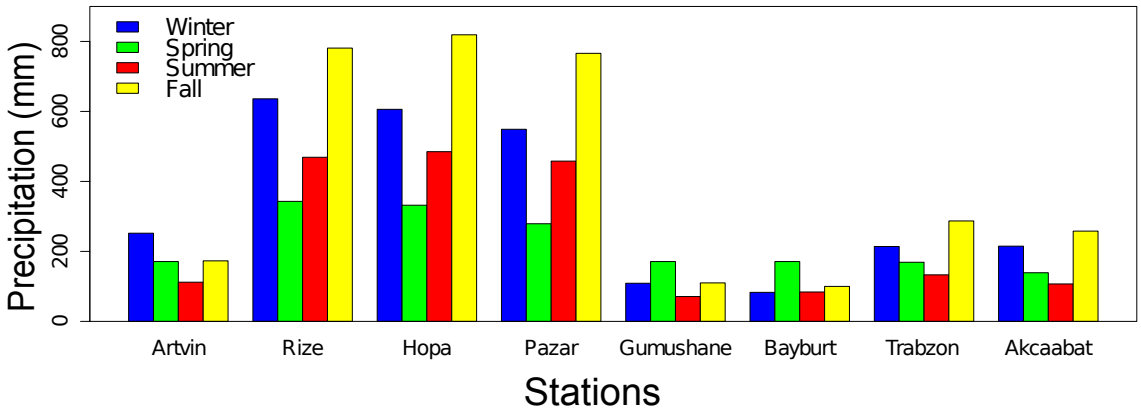

Figure 3. Long-term (1960-2014) mean of the seasonal precipitation amounts related to the eight meteorological stations in the EBS.

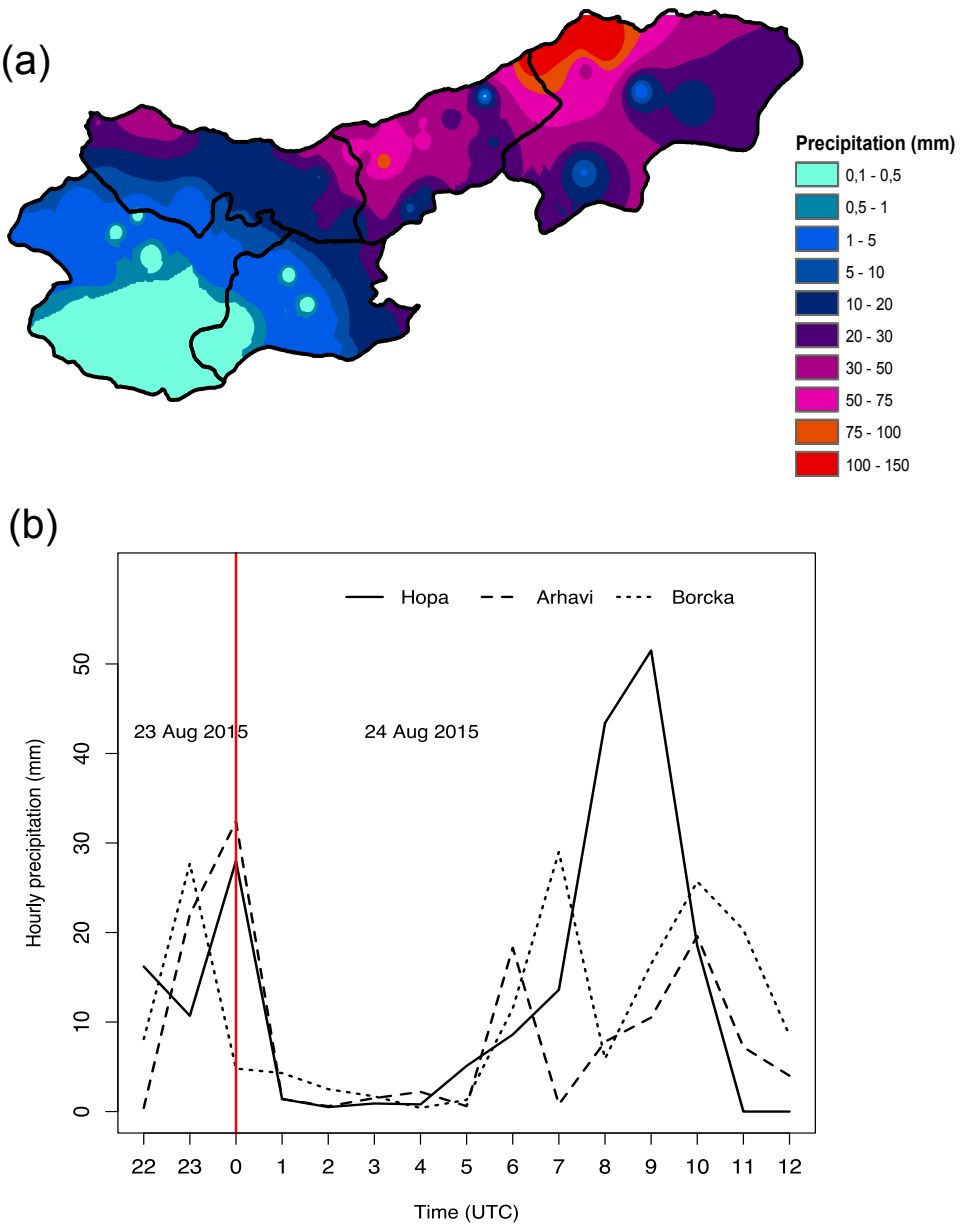

483

484 **Figure 4**. **(a)** Total daily precipitation in the eastern Black Sea (00:00-24:00 UTC), 24

485 August 2015. The map is based on data from the same meteorological stations represented

486 in Fig. 1 (station names are listed in Table 1). **(b)** Hourly evolution of the 24 August 2015

487 rainstorm in Artvin, in three selected stations representing flash-flood regions

488

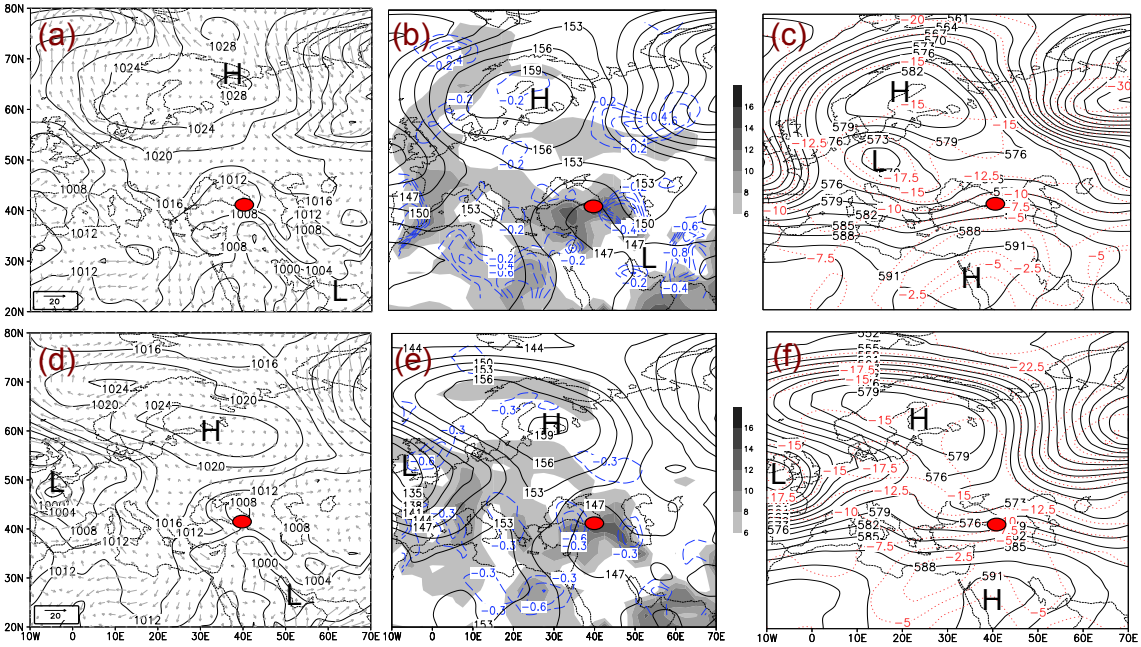

Figure 5. **(a)** Sea level pressure chart (lines, units in hPa) and surface winds (arrows, units in m s^{-1}). **(b)** Geopotential height field (units in dm), specific humidity contents (shaded in colors, units in g kg^{-1}), and moisture convergence values (dashed lines, removed positive values) of the 850-hPa level. **(c)** Geopotential height field (units in dm), and temperature values (dashed red lines in °C) of the 500-hPa level. Synoptic charts are belonging to the 23 August 2015, 00:00 UTC. The data of surface, lower and upper levels are derived from NCEP/NCAR Reanalysis. Red dot marks the studied region. **(d)** same as **(a), (e)** same as **(b), (f)** same as **(c),** but for 24 August 2015, 00:00 UTC.

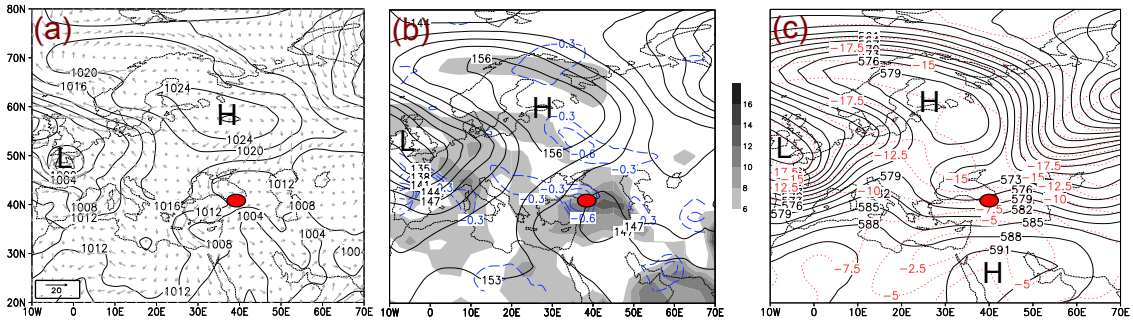

Figure 6. **(a)** same as Fig. 5(a), **(b)** same as Fig. 5(b), **(c)** same as Fig. 5(c), but for 24 August 2015, 06:00 UTC.

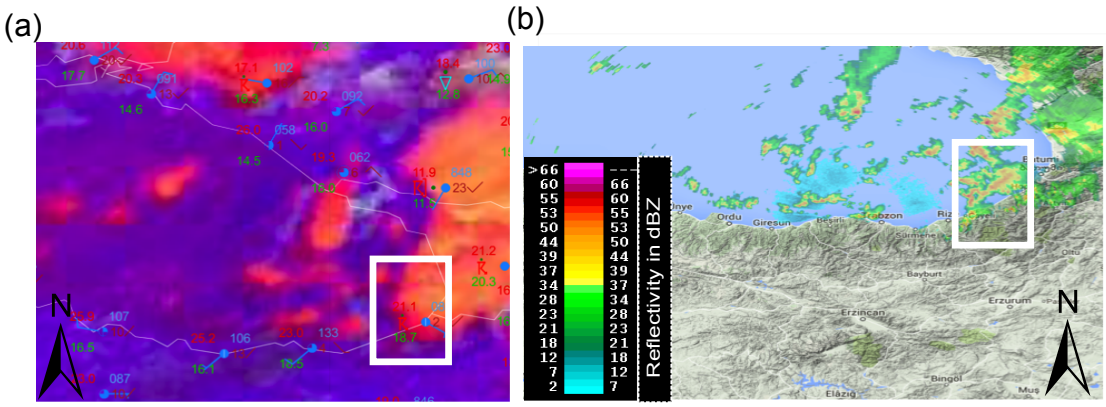

Figure 7. Satellite and radar images on 24 August 2015, 06:00 UTC. **(a)** Convective storm RGB product from SEVIRE MSG (Meteosat Second Generation) together with SYNOP observations. **(b)** Radar PPI (Plan Position Indicator) image of the EBS region. Sources: (a) EUMETRAIN (http://www.eumetrain.org/) (b) Turkish State Meteorological Service (www.mgm.gov.tr)

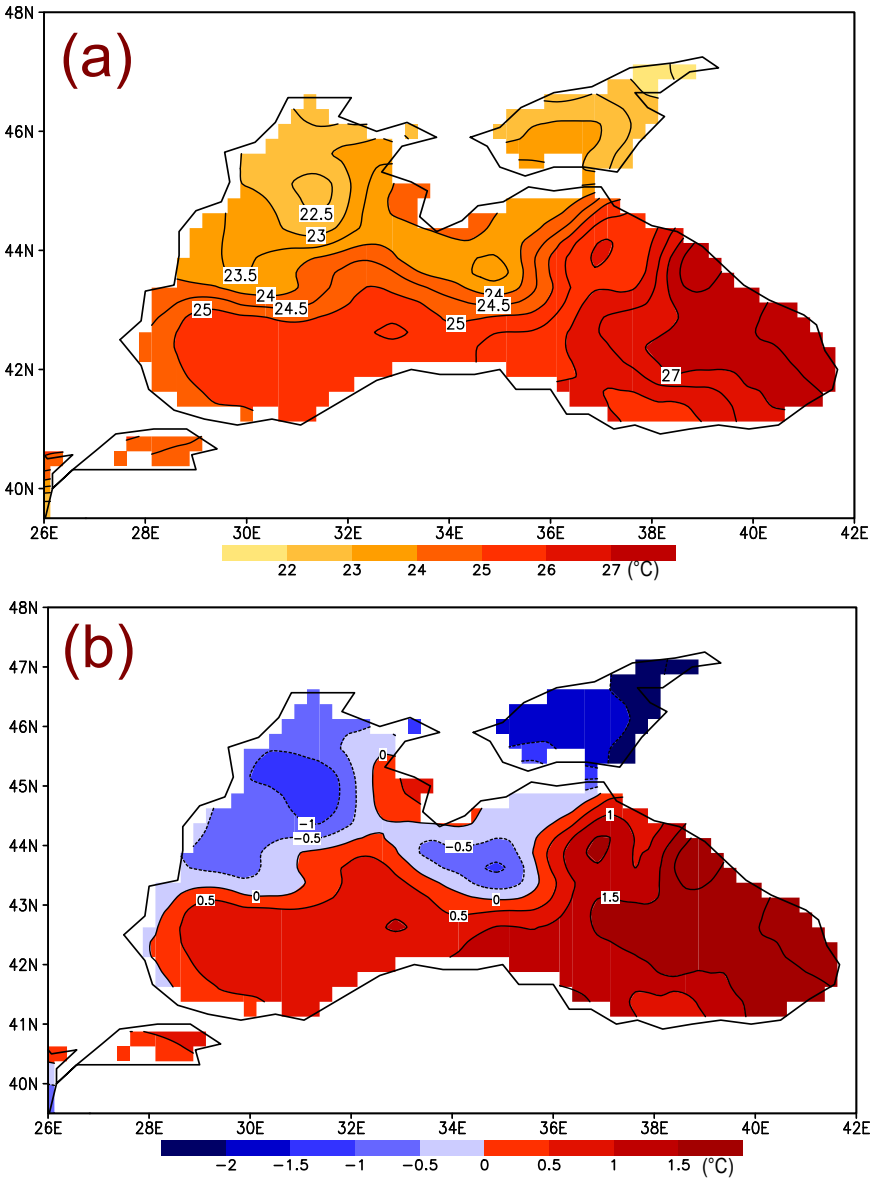

Figure 8. **(a)** Spatial distribution of the long-term (1960-2014) mean of August sea surface temperatures (SSTs) over the Black Sea. **(b)** Anomaly values of the 24 August daily mean SSTs when compared with long-term August mean SSTs. The SST Reanalysis data are derived from NOAA High Resolution SST (from their website is http://www.esrl.noaa.gov/psd).

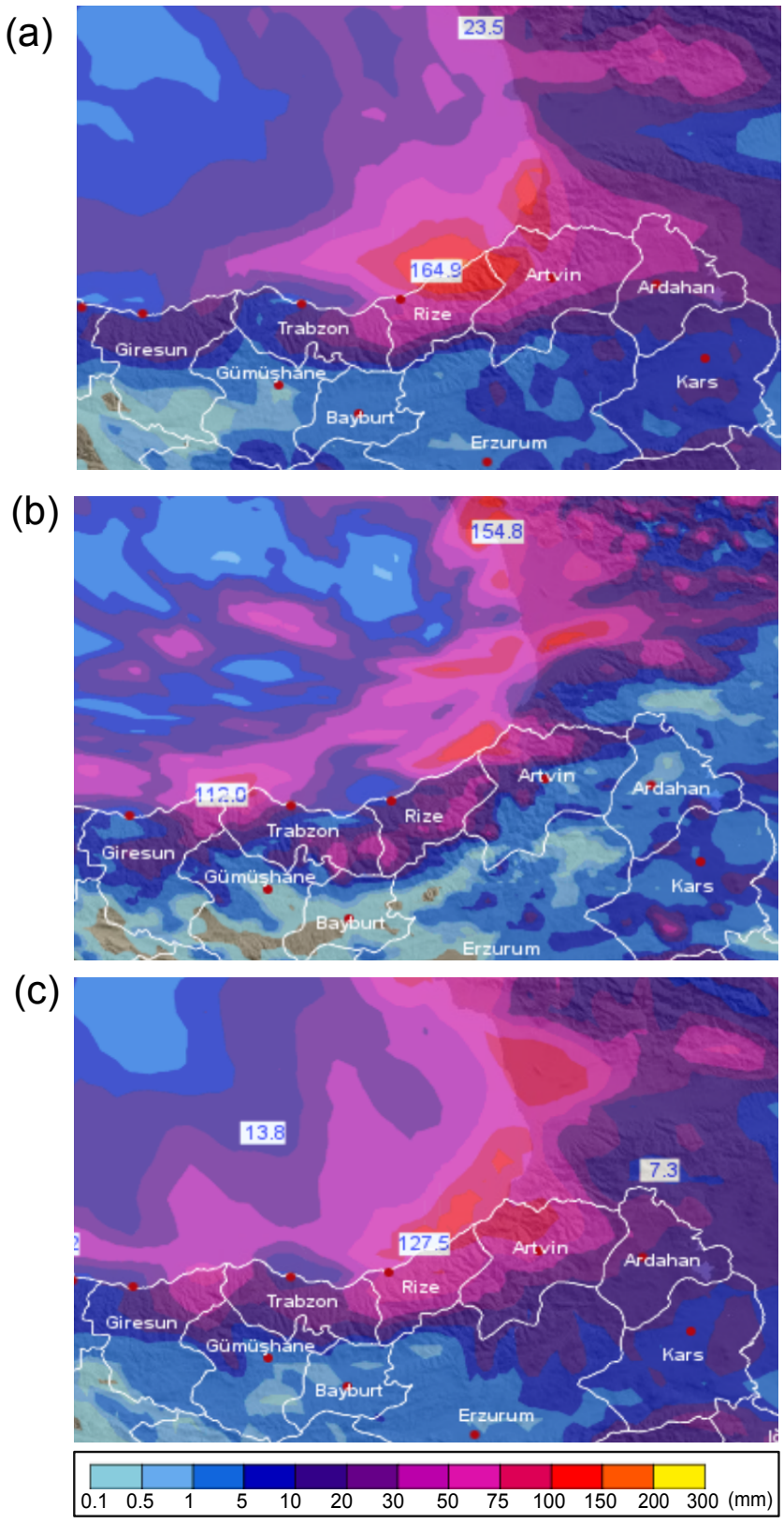
(a)
23.5
164.9
Artvin
Ardahan
Rize
Trabzon
Giresun
Gümüşhane
Kars
Bayburt
Erzurum
(b)
154.8
112.0
Artvin
Ardahan
Rize
Trabzon
Giresun
Gümüşhane
Kars
Bayburt
Erzurum
(c)
13.8
7.3
127.5
Artvin
Ardahan
Rize
Trabzon
Giresun
Gümüşhane
Kars
Bayburt
Erzurum
0.1 0.5 1 5 10 20 30 50 75 100 150 200 300 (mm)

521

522 **Figure 9**. Numerical Weather Prediction (NWP) precipitation forecasts for the 24-h daily
523 precipitation totals belonging to the 24 August 2015 in the EBS region **(a)** for ECMWF **(b)**
524 for ALARO and **(c)** for WRF. Sources: (a-c) Turkish State Meteorological Service (TSMS)

525